Lasing in an Assembled Array of Silver Nanocubes

Mindaugas Juodėnas[*1], *Nadzeya Khinevich*[1], *Gvidas Klyvis*[1],
Joel Henzie[2], *Tomas Tamulevičius*[1], *Sigitas Tamulevičius*[1]

Supplementary information

Materials and methods

Nanoparticle synthesis

Monodisperse solutions of Ag nanocubes were prepared using a modified procedure based on the polyol synthesis method described in *J. Phys. Chem. C*; **121**, 24159-24167 (2017). 80 mg of copper chloride ($CuCl_2$) was dissolved in 10 g of 1,5-pentanediol (PD; Acros). Next, 0.4 g of polyvinylpyrrolidone (PVP; Sigma-Aldrich) was dissolved in 20 g of PD by sonication. And in a separate vial, 35 µL of the above $CuCl_2$ solution and 0.4 g of $AgNO_3$ was dissolved in 20 g of PD via sonication. Next, 20 g of PD was added to a 100 mL round bottom flask (RBF) and heated to an internal temperature of 130 °C. Once the PD reached 130 °C, 500 µL of the $AgNO_3$ solution was added to the RBF, then 30 s later 500 µL of the PVP solution was added to the RBF. This procedure was repeated every minute (i.e. add the Ag+ solution at 0:00, the PVP solution at 0:30, then Ag+ at 1:00, and so forth) until the nanocubes achieved the desired size. The Ag nanocubes used in this study had an average edge length (a) of 77 ± 3 nm, measured across 200 nanoparticles using a JEOL-1010 Transmission Electron Microscope (TEM) set at 100 kV with a resolution of 0.5 nm/pixel. These particles were dispersed in DMF at a concentration of 3.59×10^{11} particles per milliliter, as confirmed by inductively coupled plasma atomic emission spectrometry. During the synthesis, each Ag nanocube is coated with a polyvinylpyrrolidone (PVP; molecular weight 55,000) surfactant layer, which acts as a steric barrier to prevent excessive aggregation when particle concentrations are high, which is key to ensure a successful deposition on templates.

Silver nanocubes produced via the polyol method are indeed single crystals, as the synthesis conditions favour uniform monocrystalline growth.[1,2] It has been proven experimentally that many single-crystal FCC metals form truncated octahedron according to Wulff's theorem.[3] However, surfactants like polyvinylpyrrolidone (PVP) alter the surface energy landscape of FCC metals because the carbonyl oxygen of the amide bond in PVP binds more strongly to facets with higher surface energy—specifically, the {100} facets—thereby stabilizing them.[4] This preferential binding suppresses growth along the <100> crystallographic directions, promoting the formation of nanocubes bounded predominantly by {100} facets. Consequently, the resulting nanocubes are single-crystalline with well-defined {100} surfaces, a fact that has been long supported in the literature[5] and even viewed in atomically resolved STEM[6] and SAED[2].

Simulations

Finite element method (FEM) modeling was performed using COMSOL Multiphysics using the wave optics module. Samples were modeled by building a unit cell with Floquet boundary conditions. The array was illuminated from a port below the nanoparticles; a second port above collected the transmitted light. The dielectric function was used from Johnson & Christy data.[7]

Fabrication of the SLR-based resonator

Capillary-assisted particle assembly deposition on PDMS replica was performed using a custom setup equipped with a motorized linear precision translator (LS-110, PI Micos), a temperature control system (TEC-1090, Meerstetter Engineering GmbH), and an optical microscope system (BX51, Olympus) with a CCD camera (Micropublisher 3.3, QImaging). The PDMS templates are produced by molding the structure from a silicon master nanofabricated using e-beam lithography (eLine Plus, Raith) and inductively coupled plasma reactive ion etching (Apex SLR, Plasma-Therm). The templates were placed on the moving stage, and 100 µl of silver nanocube solution was injected and confined by a fixed microscope slide. The drop of solution moved along the surface with a stage speed of 3.3 µm/s, forming the meniscus. Evaporation-induced flux and the contact angle led to nanocubes accumulating at the edge of the meniscus and filling the traps. The temperature of the sample holder is controlled by the thermoelectric controller and was set at 13.2°C above the dew point.

Nanolaser architecture

To realize lasing emission from these NP cavities, we used pyrromethene 597 dye (Exciton) as gain material. The dye was dissolved in DMSO:Ethanol in a ratio of 2:1 to achieve index matching at n=1.42. The concentration of the dye was 5 mM. The nanoparticle arrays were submerged into this solution to allow the dye to penetrate PDMS and surround the nanoparticles. Before experiments, a drop of dye solution (10 µl) was placed on the substrate and covered by a glass cover slip.

Nanolasing measurements

The nanolaser was pumped by the 2nd harmonic (515 nm) of 290 fs pulse length Yb:KGW laser Pharos (Light Conversion) at a 40 kHz repetition rate at room temperature. The pulse picker was set to transmit every 800th pulse to effectively reduce the frequency to 50 Hz. The pump beam was reduced to a 1.4 mm FWHM diameter spot (2.38 mm 1/e^2) on the sample at an incident angle of *ca.* 22°. The emission spectra were collected at the normal to the sample surface using a home-built experimental setup. Optical characterization of the fabricated template demonstrated SLR and lasing emission were registered using a fiber-optic spectrograph AvaSpec-2048 (Avantes) with a 1.2 nm resolution in the 400–800 nm spectral range. The spatial pattern and divergence angle of the lasing beam were analyzed using a beam profiler WinCamD-LCM (DataRay Inc.) equipped with a 1” CMOS sensor and placed normal to the sample surface on an optical rail.

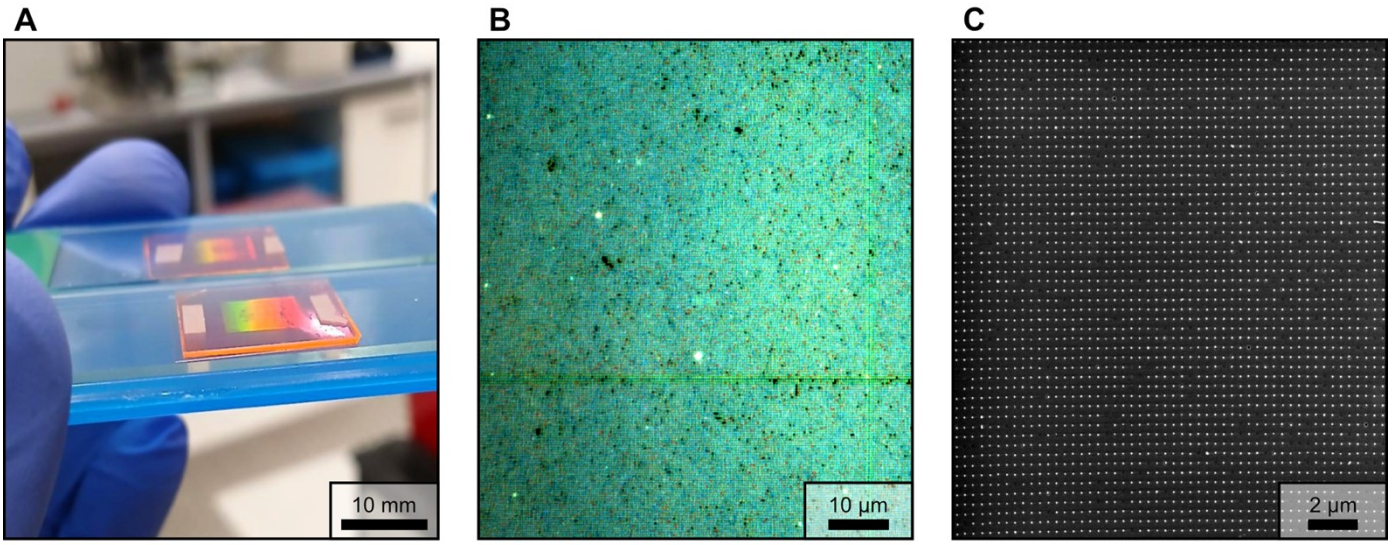

Figure S1. Templated self-assembly scalability. A) Camera image of an assembled nanolaser. B) Optical dark-field image and C) SEM image of the assembled nanocubes in a 400 nm square lattice.

Table S1. Summary of the characteristics of SLR-based nanolasers with similar architectures to the one presented in this work ranked according to the lasing threshold

Wavelength, nm	**Threshold, μJ/cm²**	**Period, nm**	**Material**	**Gain Medium**	**Pumping**	**Year**	**Ref.**
574	80	400	Ag	Pyrromethene 597	515 nm, 290 fs	2024	This work
883	60-120	600	Au	IR-140	800 nm, 35 fs	2019	[8]
862-891	95-188	600	Au	IR-140	800 nm, 90 fs	2015	[9]
862	110	600	Au	IR-140	800 nm, 150 fs	2017	[10]
580	180	400	Al	C540a	400 nm, 100 fs	2023	[11]
868	200	346	Ag	IR-140	800 nm, 35 fs	2022	[12]
913	230	600	Au	IR-140	800 nm, 40fs	2013	[13]
886	250	580	Au	IR-792	792 nm, 150 fs	2021	[14]
871	300	600	Au	IR-140	800 nm, 90 fs	2018	[15]
897	317	590	Au	IR-140	800 nm, 100 fs	2022	[16]
657	500	225	Al	DCM	400 nm, 35 fs	2021	[17]
511	510	350	Al	C500	400 nm, 100 fs	2021	[18]
651	570	450	Al	DCM	400 nm, 100 fs	2021	[18]
466	740	450	Al	C480	400 nm, 100 fs	2021	[18]
567	820	375	Ag	Rhodamine 6G	500 nm, 100 fs	2017	[19]

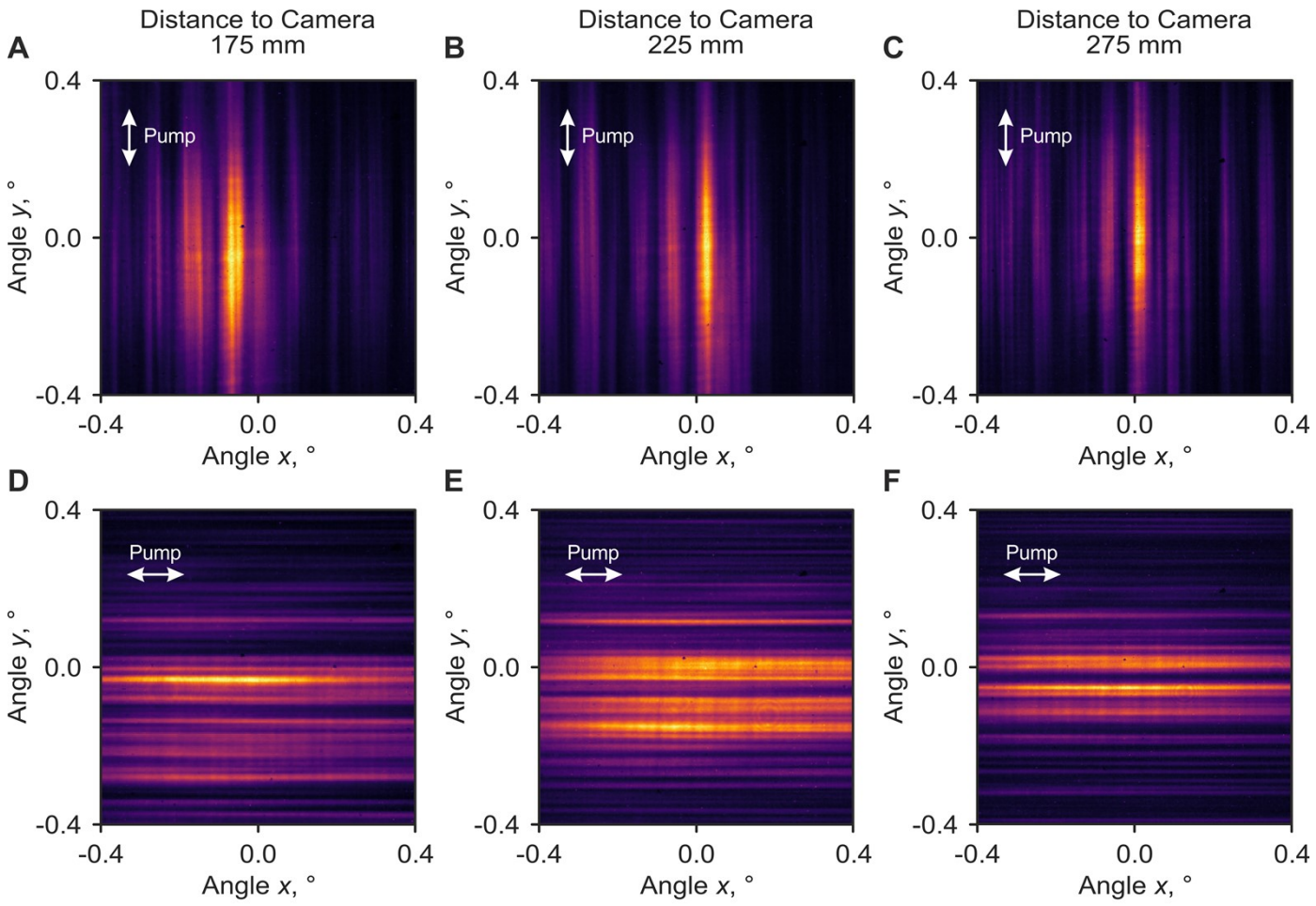

Figure S2. Camera images of the emitted beam were taken at varying distances from the nanolaser (indicated above), and two characteristic polarizations are indicated in the top left of each image.

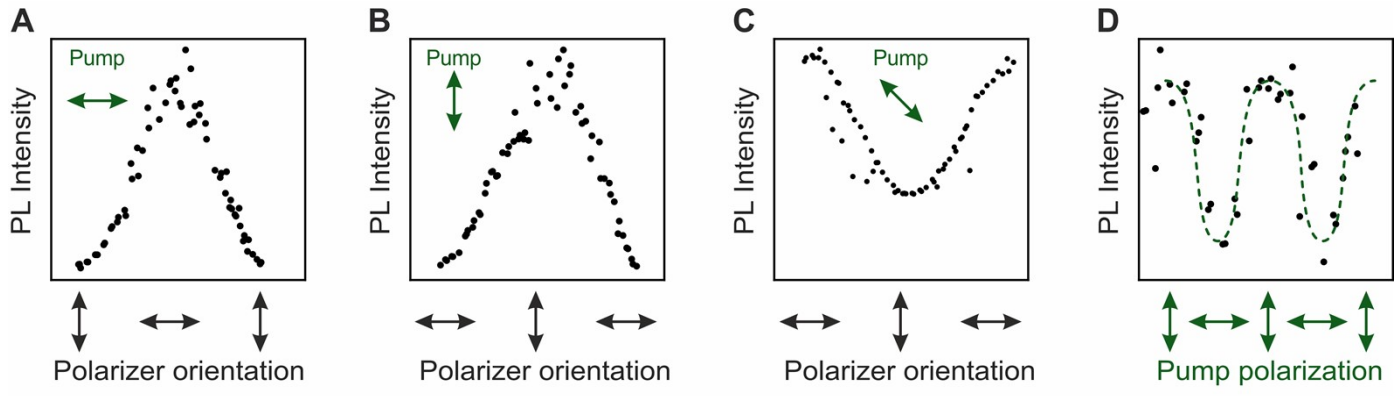

Figure S3. The polarization of the emitted beam was characterized by placing a linear polarizer between the nanolaser and the spectrometer. Measurements were done by rotating the polarizer when pumping with TM (a), TE (b), and 45° (c) polarized light. Finally, the polarizer after the nanolaser was removed and the polarization of the pump was rotated continuously (d).

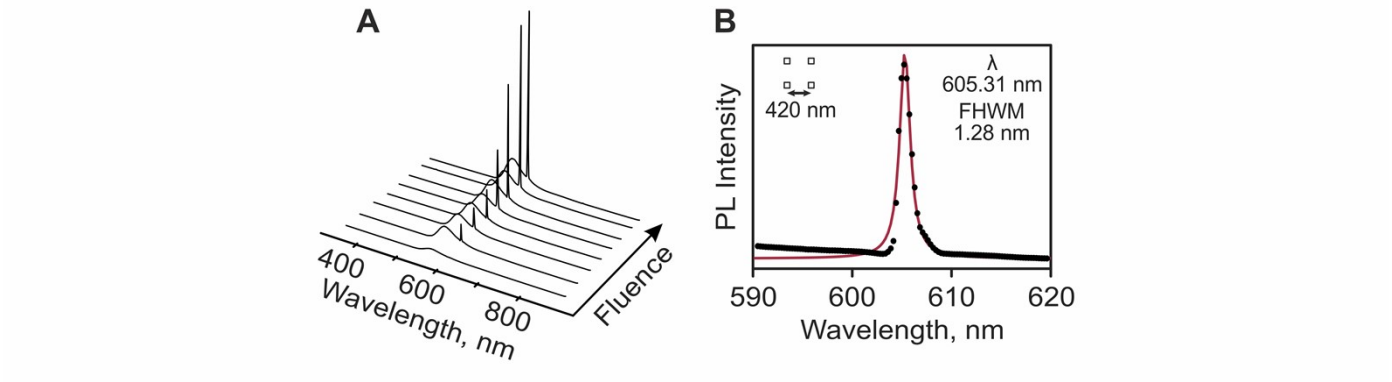

Figure S4. Nanolaser emission with a 420 nm periodicity SLR system. The device shows threshold behavior and linewidth narrowing (a), and emission is centered at 605 nm (b), consistent with the change of the flat band shift (RA is calculated at 420 nm x 1.42 = 596.4 nm)

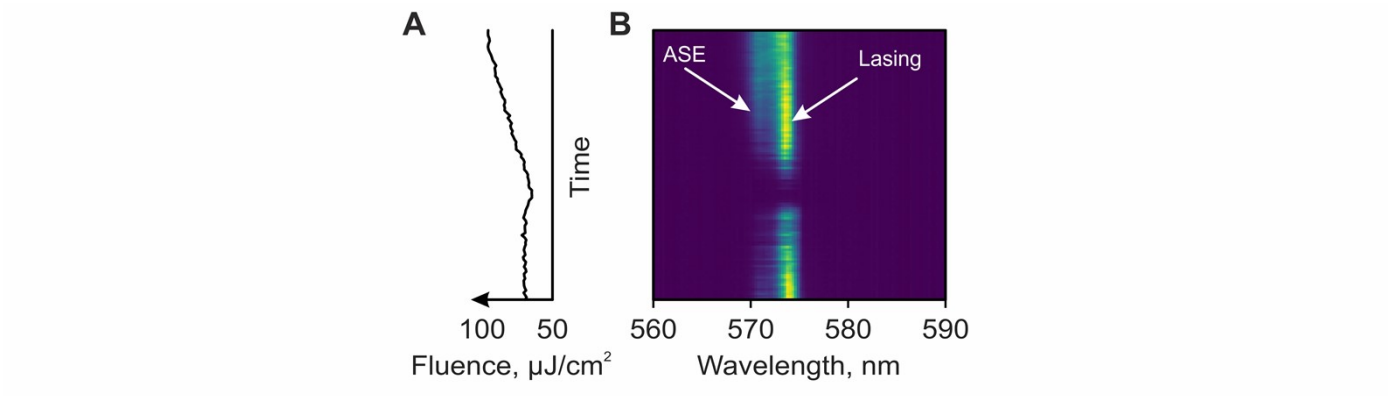

Figure S5. In some cases, higher intensity pumping (a) results in the rise of amplified spontaneous emission as a broader shoulder next to the lasing peak (b).

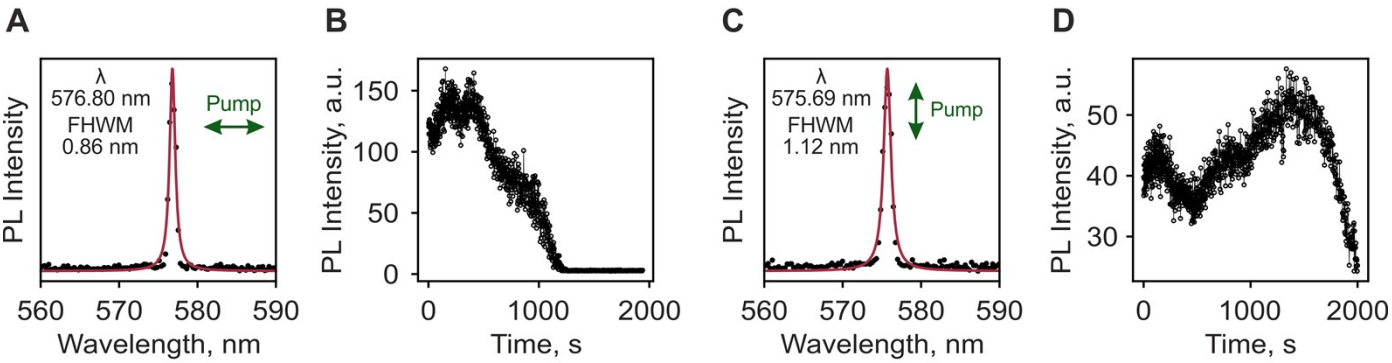

Figure S6. Long-term measurement of the nanolaser using orthogonal polarizations. a, b) TM polarization, the device lased for ~1000 s; c, d) TE polarization, the device lased for >2000 s, albeit at a lower intensity.

1. Zhou, S. *et al.* Facile Synthesis of Silver Nanocubes with Sharp Corners and Edges in an Aqueous Solution. *ACS Nano* **10**, 9861–9870 (2016).
2. Sun, Y. & Xia, Y. Shape-Controlled Synthesis of Gold and Silver Nanoparticles. *Science* **298**, 2176–2179 (2002).
3. Marks, L. D. Experimental studies of small particle structures. *Rep. Prog. Phys.* **57**, 603 (1994).
4. Borodko, Y. *et al.* Probing the interaction of poly(vinylpyrrolidone) with platinum nanocrystals by UV-Raman and FTIR. *J. Phys. Chem. B* **110**, 23052–23059 (2006).
5. Xia, Y., Xiong, Y., Lim, B. & Skrabalak, S. E. Shape-controlled synthesis of metal nanocrystals: simple chemistry meets complex physics? *Angew. Chem. Int. Ed Engl.* **48**, 60–103 (2009).
6. Matteini, P. *et al.* Site-Selective Surface-Enhanced Raman Detection of Proteins. *ACS Nano* **11**, 918–926 (2017).
7. Johnson, P. B. & Christy, R. W. Optical Constants of the Noble Metals. *Phys. Rev. B* **6**, 4370–4379 (1972).
8. Wang, W. *et al.* Ultrafast Dynamics of Lattice Plasmon Lasers. *J. Phys. Chem. Lett.* **10**, 3301–3306 (2019).
9. Yang, A. *et al.* Real-time tunable lasing from plasmonic nanocavity arrays. *Nat. Commun.* **6**, 6939 (2015).
10. Hoang, T. B., Akselrod, G. M., Yang, A., Odom, T. W. & Mikkelsen, M. H. Millimeter-Scale Spatial Coherence from a Plasmon Laser. *Nano Lett.* **17**, 6690–6695 (2017).
11. Guan, J. *et al.* Far-field coupling between moiré photonic lattices. *Nat. Nanotechnol.* 1–7 (2023) doi:10.1038/s41565-023-01320-7.
12. Juarez, X. G. *et al.* M-Point Lasing in Hexagonal and Honeycomb Plasmonic Lattices. *ACS Photonics* **9**, 52–58 (2022).
13. Zhou, W. *et al.* Lasing action in strongly coupled plasmonic nanocavity arrays. *Nat. Nanotechnol.* **8**, 506–511 (2013).
14. Asamoah, B. O. *et al.* Polarization dependent beaming properties of a plasmonic lattice laser. *New J. Phys.* **23**, 063037 (2021).
15. Wang, D. *et al.* Stretchable Nanolasing from Hybrid Quadrupole Plasmons. *Nano Lett.* **18**, 4549–4555 (2018).
16. Heilmann, R., Salerno, G., Cuerda, J., Hakala, T. K. & Törmä, P. Quasi-BIC Mode Lasing in a Quadrumer Plasmonic Lattice. *ACS Photonics* **9**, 224–232 (2022).
17. Guan, J. *et al.* Identification of Brillouin Zones by In-Plane Lasing from Light-Cone Surface Lattice Resonances. *ACS Nano* **15**, 5567–5573 (2021).
18. Guan, J. *et al.* Plasmonic Nanoparticle Lattice Devices for White-Light Lasing. *Adv. Mater.* **35**, 2103262 (2023).
19. Hakala, T. K. *et al.* Lasing in dark and bright modes of a finite-sized plasmonic lattice. *Nat. Commun.* **8**, 13687 (2017).